BOREAL ENVIRONMENT RESEARCH 21: 481–503
ISSN 1239-6095 (print) ISSN 1797-2469 (online)

Helsinki 11 May 2016

Soot-doped natural snow and its albedo — results from field experiments

Jonas Svensson[1)]*, Aki Virkkula[1)2)3)], Outi Meinander[1)], Niku Kivekäs[1)4)], Henna-Reetta Hannula[5)], Onni Järvinen[3)], Jouni I. Peltoniemi[3)6)], Maria Gritsevich[6)3)7)], Anu Heikkilä[1)], Anna Kontu[5)], Kimmo Neitola[1)], David Brus[1)], Pavla Dagsson-Waldhauserova[8)9)10)], Kati Anttila[1)6)], Marko Vehkamäki[11)], Anca Hienola[1)], Gerrit de Leeuw[1)3)] and Heikki Lihavainen[1)]

[1)] *Finnish Meteorological Institute, P.O. Box 503, FI-00101 Helsinki, Finland (*corresponding author's e-mail: jonas.svensson@fmi.fi)*
[2)] *Institute for Climate and Global Change Research & School of Atmospheric Sciences, Nanjing University, 163 Xianlin Road, CN-210023 Nanjing, China*
[3)] *Department of Physics, P.O. Box 64, FI-00014 University of Helsinki, Finland*
[4)] *Department of Physics, Lund University, P.O. Box 118, SE-221 00 Lund, Sweden*
[5)] *Arctic Research Center, Finnish Meteorological Institute, Tähteläntie 62, FI-99600 Sodankylä, Finland*
[6)] *Finnish Geospatial Research Institute, Geodeetinrinne 2, FI-02430 Masala, Finland*
[7)] *Institute of Physics and Technology, Ural Federal University, RU-620002 Ekaterinburg, Russia*
[8)] *Faculty of Environment, Agricultural University of Iceland, Hvanneyri, IS-311 Borgarnes, Iceland*
[9)] *Departments of Physical and Earth Sciences, University of Iceland, Sæmundargata 2, IS-101 Reykjavik, Iceland*
[10)] *Czech University of Life Sciences Prague, Faculty of Environmental Sciences, Department of Ecology, Kamycka 1176, CZ-165 21, Prague, Czech Republic*
[11)] *Department of Chemistry, P.O. Box 55, FI-00014 University of Helsinki, Finland*

Received 23 Dec. 2015, final version received 6 Apr. 2016, accepted 7 Apr. 2016

Svensson J., Virkkula A., Meinander O., Kivekäs N., Hannula H.-R., Järvinen O., Peltoniemi J.I., Gritsevich M., Heikkilä A., Kontu A., Neitola K., Brus D., Dagsson-Waldhauserova P., Anttila K., Vehkamäki M., Hienola A., de Leeuw G. & Lihavainen H. 2016: Soot-doped natural snow and its albedo — results from field experiments. *Boreal Env. Res.* 21: 481–503.

Soot has a pronounced effect on the cryosphere and experiments are still needed to reduce the associated uncertainties. This work presents a series of experiments to address this issue, with soot being deposited onto a natural snow surface after which the albedo changes were monitored. The albedo reduction was the most pronounced for the snow with higher soot content, and it was observed immediately following soot deposition. Compared with a previous laboratory study the effects of soot on the snow were not as prominent in outdoor conditions. During snowmelt, about 50% of the originally deposited soot particles were observed to remain at the snow surface. More detailed experiments are however needed to better explain soot's effect on snow and to better quantify this effect. Our albedo *versus* soot parameterization agreed relatively well with previously published relationships.

Editor in charge of this article: Veli-Matti Kerminen

Introduction

Soot particles consist of black carbon (BC) and organics, originating from both anthropogenic and natural combustion sources. Once deposited onto snow surfaces, they increase absorption of solar radiation and reduce the snow's albedo (Warren and Wiscombe 1980). This leads to faster snow aging, resulting in further lowered reflectivity. With more aged snow, the effect of BC on snow and ice is further enhanced. This positive feedback leads to an earlier onset of snowmelt (Flanner *et al*. 2007).

Ambient measurements of BC in snow and ice have been conducted in different regions of the globe. For example, in the Arctic, BC concentrations in snow have been shown to be in the range of 0–100 ppb (Forsström *et al*. 2009, 2013, Doherty *et al*. 2010, Meinander *et al*. 2013, Svensson *et al*. 2013) and cause a perturbation to the radiative balance (Flanner *et al*. 2007). In Himalayan snow and ice, with a closer proximity to major emission sources, higher BC concentrations (> 100 ppb) have been measured and have been proposed to have a more pronounced negative effect on the cryosphere and the hydrological cycle (e.g., Xu *et al*. 2012, Kaspari *et al*. 2014, Qu *et al*. 2014). The same has also been observed in the snow of the European Alps (e.g. Fily *et al*. 1997, Lavanchy *et al*. 1999). However, there were only few experimental studies of the effect of BC on snow (Conway *et al*. 1996, Brandt *et al*. 2011, Hadley and Kirchstetter 2012).

Conway *et al*. (1996) mixed high amounts (0.003–0.03 kg m^{-2}) of soot (both of hydrophilic and hydrophobic character) and volcanic ash in 10 liters of snow and distributed these separate contaminant mixtures in a 2.5-cm-deep layer on top of the melting snow during the melt season on the Blue Glacier, WA, USA. Thereafter, the ablation and albedo were monitored and it was found that during the melt, the soot particles were more efficiently scavenged through the snow than the volcanic-ash particles. The soot particles were of submicron size while the volcanic ash particles were larger (> 5 μm), probably explaining the difference in scavenging efficiency. Additionally, the hydrophobic soot particles were less efficiently scavenged through the snow than the hydrophilic soot particles. Nonetheless, the remaining fraction of soot particles at the surface still caused a clear reduction in albedo (30% less for the contaminated snow compared to the natural snow) and an increase in ablation rate of 50% on the glacier surface, compared to the non-contaminated glacier surface.

The experimental approach used by Brandt *et al*. (2011) was based on two artificial snowpacks (with and without added soot) created with a snow gun on an open field. Snow samples were collected and analyzed for their BC concentration with a filter-based method (filters analyzed optically). With the combined BC concentration and the inferred snow grain size based on near-infrared albedo measurements, they calculated the albedo reduction of the snowpack in a radiative transfer model, confirming the negative effect of BC on the snowpack albedo.

Hadley and Kirchstetter (2012) produced pure and BC contaminated artificial snowpacks in a laboratory experiment to study the effects of BC on snow albedo. With BC concentrations in a wide range, BC was found to reduce snow albedo, with the BC effects amplified when the snow grain size was increased. This study also verified the widely used Snow, Ice and Aerosol Radiation (SNICAR) model (Flanner *et al*. 2007).

While Conway *et al*. (1996) focused on the mobility of soot and ash particles through the snowpack during glacier melt, using very high concentrations of impurities on the snow; Brandt *et al*. (2011) contaminated snow with 2500 ppb BC and had its albedo reduction verified in a radiative transfer model. Hadley and Kirchstetter (2012) used a range of different BC levels and snow grain sizes to confirm the reduction of BC on snow albedo in a controlled laboratory environment.

Here, we present a series of unique experiments, carried out during three consecutive winters in different regions of Finland, in which we deposited soot onto a natural snowpack. The idea was to deposit the soot in a controlled way and thereafter measure the snow albedo and monitor it throughout the melting season. Selected observations of the snow physical properties and the temporal progression of soot concentrations were also conducted. The first results of these

experiments were presented by Meinander *et al*. (2014) who showed that the BC affects the density of melting snow and by Peltoniemi *et al*. (2015) who showed that the reflectance of the soot-doped snow has a strong directional dependence. While these two papers presented selected, focused results from these experiments, the goal of the present paper is to give an overview of all the experiments, including time series of the observations, highlighting albedo and recommendations for planning future experiments based on the experiences gained.

Experiments and methods

Experiment sites

The experiments were conducted in three consecutive winters: 2011, 2012, and 2013. In 2011, they were undertaken from early March until April on a farming field in southern Finland (60°24´N, 24°42´E) near the town of Nurmijärvi, 30 km north of Helsinki. When the experiment commenced, the snowpack thickness was 50 cm and winter conditions with subzero temperatures prevailed in the area. The second experiment was conducted in another farming field at the Finnish Meteorological Institute (FMI) observatory (60°48´N, 23°30´E) in Jokioinen, southern Finland, ~100 km northwest of Helsinki, in February and March. At the start of the experiment, the snow depth at the site was 30 cm. The third experiment took place at the Sodankylä airfield (67°23´N, 26°36´E), located near the FMI Arctic Research Centre, in Sodankylä, northern Finland, in April and May 2013. The snow depth at the experimental site was 65 cm before the soot deposition started. Hereafter, the experiments in 2011, 2012, and 2013 will be referred to as SoS2011, SoS2012, and SoS2013, respectively.

Soot deposition onto the snow

Soot was deposited with different methods onto the snow surface (*see* Table 1). During SoS2011, soot particles were produced by burning various organic materials (wood and rubber pellets from used tires) in a wood-burning stove. The smoke was led through a pipe, cooled by snow surrounding the pipe, and into a rectangular chamber (3.3 × 7.5 × 2.8 m, W × L × H) standing on top of the snow (Fig. 1A). The air in the smoke was not cooled enough before entering the chamber, thus a majority of the particles escaped the chamber with the warmer air and were not deposited in the desired location on the snow. According to infrared images taken during the burning, the temperature of the surface snow inside the chamber remained below freezing (Fig. 1B), hence, melting did not occur during the soot deposition. Inside the chamber, the soot particles were deposited onto the snow surface in a heterogeneous pattern (Fig. 1C). An undisturbed reference site, with no impurities added, was established in close proximity (15 m) to the experimental chamber.

Because of the temperature gradient and the heterogeneous distribution pattern of the deposited soot particles in SoS2011, a different approach to deposit the soot was taken in SoS2012 and SoS2013. Soot was acquired beforehand from a chimney-sweeping company (Consti Talotekniikka) in Helsinki, which collected the soot from residential buildings with small-scale wood and oil burning. The soot was blown into a custom-made cylindrical chamber (diameter of 4 m) that was carefully placed on the snow surface. The blowing system consisted of a blower, a tube blowing air into a barrel filled with the soot, and a cyclone removing particles larger than about 3 μm (Fig. 2A). Since the flow did not remain constant during the blowing, the removal of larger particles with the cyclone was only achieved with moderate success, as was observed in the electron microscopic analyses (*see* section "Electron microscopic analyses").

After the deposition of soot in SoS2012, the three soot-contaminated spots were covered with 10 cm of new snow. The sensors had not even been set up to measure albedos of clean and soot-doped snow before the snowfall started. The following day high winds occurred as well. After these events all of the spots had very similar albedos and the melting time of the snow depended mostly on the amount of snow on each spot. The soot analysis of the snow samples revealed that samples collected one month later contained significantly four times less soot as

Table 1. General characteristics of SoS2011 and SoS2013 campaigns and the measurements performed. (**A**) SoS 2011, Nurmijärvi, southern Finland, 5 March 2011–12 April 2011: soot produced by burning organics in a stove was deposited onto snow surface in rectangular chamber; (**B**) SoS 2013, Sodankylä, northern Finland, 4 April 2013–2 May 2013: soot collected from a chimney was deposited onto several spots on the snow surface through a blowing system.

	Elemental carbon analysis of snow samples	Albedo	Snow stratigraphy, including: hardness, wetness, density, grain size, and shape, and temperature	Meteorological observations
A				
Date	5 March 2011	Broadband measurements continuous	1 April 2011	Continuous
Comments	Surface samples collected following soot deposition	–	Snow-pit measurements of reference snow and sooted snow area	–
Results presented in this paper	Table 2, section "Elemental carbon in SoS2013 surface snow"	Fig. 4a, section "SoS2011"	Appendixes 1–2, section "Physical snow characteristics"	Fig. 4a
B				
Date	4 April 2013–8 April 2013, 17 April 2013	Broadband measurements continuous	3 April 2013, 5 April 2013, 6 April 2013, 10 April 2013, 17 April 2013	Continuous
Comments	Sampling of all spots immediately following soot deposition; sampling of spots S5, S7, and reference area on 17 April	–	Reference snow-pit measurements on 3, 5 and 6 April; snow pits of sooted snow spots S5 and S7 on 10 April; snow pits of S5, S7 and reference snow* on 17 April	–
Results presented in this paper	Table 2, section "Elemental carbon in SoS2013 surface snow"	Fig. 4b, section "SoS2013"	Appendixes 3–10, section "Physical snow characteristics"	Fig. 4b

* reference snow location was moved due to contamination of original reference spot during soot deposition.

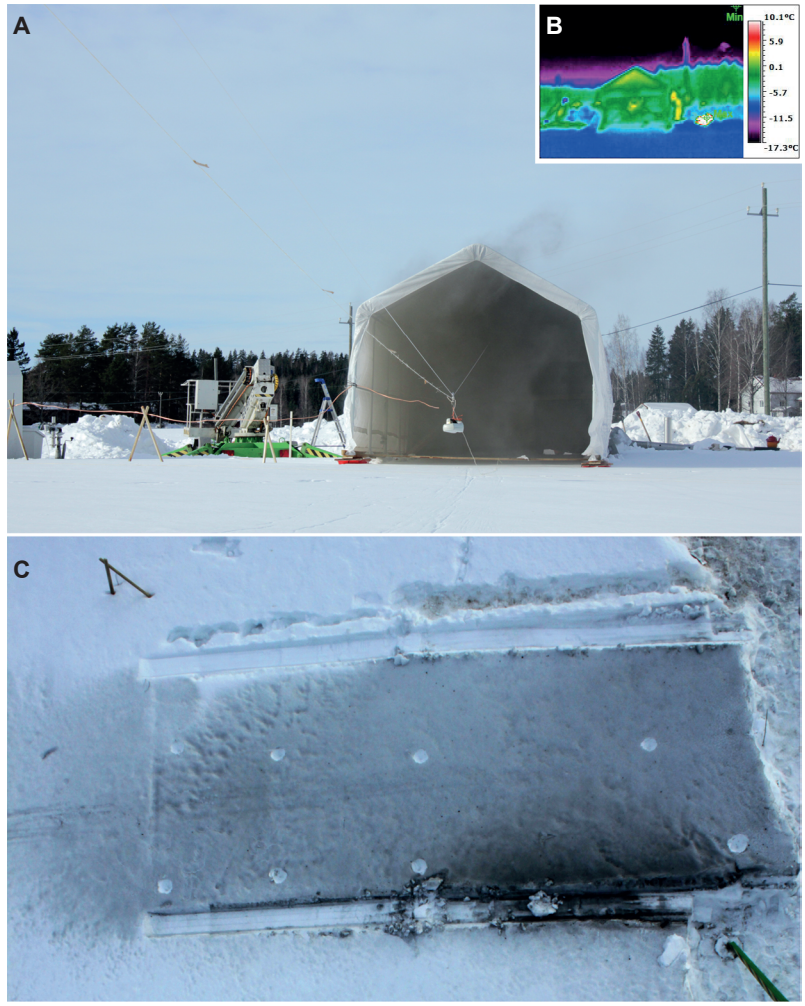

Fig. 1. Experimental set-up in SoS2011. (**A**) Soot production and deposition chamber, (**B**) thermographic infrared image of the temperature ranges during deposition, and (**C**) rectangular soot spot after removing the chamber (overhead view).

compared with the snow samples collected right after the soot deposition. We hypothesize that the snow storm removed part of the top layer, which contained the deposited soot, and therefore no clear effects of soot on snow were observed. Because of the lack of quantitative information on the soot concentration, the measurements from SoS2012 could not be analyzed and interpreted in detail, and are therefore not presented in this paper. The above description is presented here, however, to stress the importance of planning an experiment.

In 2013, several spots were made with varying amounts of soot originating from wood-burning soot (Fig. 2B), one spot by using soot from a peat-burning power plant, one spot by using soot from a residential oil burner, two spots by using glaciogenic silt from Iceland and one spot by using volcanic ash from Iceland (Fig. 2C). After depositing the impurities, pyranometers were set up above the spots (Fig. 2B) as will be described below. One spot was planned to be left as a reference spot with no added soot but it got contaminated during the soot deposition of the other spots in the afternoon of 8 April (named Ref in Table 2), which was the fifth day of measurements. A new reference site, inside the airfield, was therefore created for the post-deposition monitoring. However, no pyranometers were available for this new reference site so there are no continuous albedo data from clean reference snow in SoS2013. The spots with no albedo measurements (Fig. 2C) were created in order to make the physical characterization of

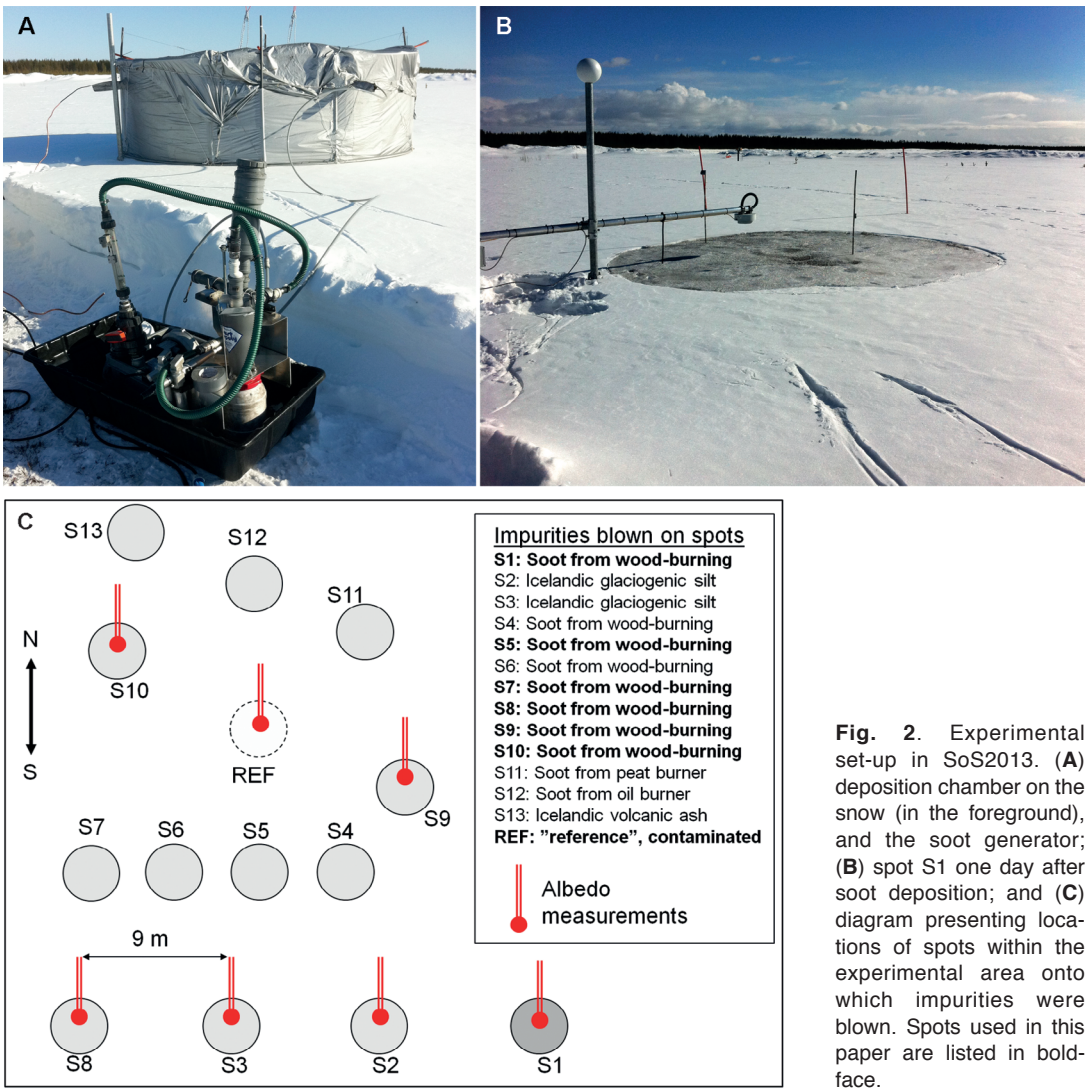

Fig. 2. Experimental set-up in SoS2013. (**A**) deposition chamber on the snow (in the foreground), and the soot generator; (**B**) spot S1 one day after soot deposition; and (**C**) diagram presenting locations of spots within the experimental area onto which impurities were blown. Spots used in this paper are listed in boldface.

Table 2. Surface snow samples and the corresponding EC concentrations, [EC], from SoS2011 and SoS201, including also the spatial variability of [EC] from each measured area or spot, depending on experiment; n/a = no albedo measurements conducted for this spot.

	Number of samples	Average [EC] (ng g^{-1})	[EC] variation (%)	Albedo after soot deposition
SoS2011				
Sooted snow area	10	20900	25	0.52
Reference snow area	6	80	39	0.83
SoS2013, spot number				
1	3	6420	35	0.41
8	4	489	40	0.75
9	4	1030	20	0.70
10	4	232	28	0.77
Ref	2	554	22	0.75
Background sample	1	46		n/a

snow and to enable snow samples to be gathered for analysis of soot content. This requires digging in the snow which would seriously affect albedo measurements. Therefore, it was planned to make duplicate spots with similar amounts of soot and set up the albedo measurement on one of the two. However, due to undetermined losses in the particle blower it turned out that it was not possible to make two spots with similar amounts of soot. The unknown losses made it also impossible to estimate the amount of glaciogenic silt and volcanic ash blown on spots S2, S3, and S13. Even though the original goal of SoS2013 was to also study the effects of the other impurities, only the effects of soot obtained from the wood-burning is discussed in the present paper.

Measurements of albedo, elemental carbon, and physical characteristics of the snow pack

Albedo measurements

Following the deposition of soot at the designated spots, albedo measurements were set up using a set of pyranometers measuring global irradiance (radiant flux in W m^{-2}) with a nominal viewing angle of 2π steradians. One of the pyranometers was installed horizontally looking upwards to measure the downwelling irradiance. Another ones, above each deposition spot, were installed horizontally looking downwards and hence recording the upwelling irradiance. In addition, one pyranometer was installed to measure the upwelling irradiance over pure snow. The albedo at each measuring spot was derived as the ratio of the upwelling to the downwelling irradiance. The pyranometers were set 30 cm above the snow surface and were thereafter lowered as snow melted throughout the experiment to maintain the same height above the snow surface. Determination of the height of the sensor was based on the requirement that the potential specular component of the reflection should emanate from the deposited surface throughout most of the day, i.e., at solar zenith angles < 80°.

The pyranometers employed in SoS2011 and in SoS2013 were CM11 and CMP6 sensors, respectively, manufactured by Kipp & Zonen B.V. The spectral range of the CM11 covers the wavelengths from 310 nm to 2800 nm, while the CMP6 covers the wavelengths from 285 nm to 2800 nm, with the spectral response close to unity throughout the whole wavelength range. Following the classification given by ISO9060:1660 (1990), CM11 and CMP6 sensors comply with the specifications defined for the secondary standards and first class instruments, respectively. In the classification defined by WMO/CIMO (WMO 2012), CM11 belongs to the category of "high quality", and CMP6 to the category of "good quality". The scale of the pyranometers used in the campaigns is traceable to World Radiometric Reference (WRR). Detailed uncertainty budgets were derived for every sensor following the guidelines given by ISO GUM (JCGM 2008), the specifications provided by ISO9060:1660 (1990) standard, and the procedure described by Kratzenberg *et al.* (2006). As a result, the expanded standard (2σ) uncertainty for CM11 sensors was found to be ±2.8% and for CMP6 sensors ±6.0%–6.1%.

The cosine response of the CM11 and CMP6 sensors is close to an ideal cosine at solar elevation angles < 10°. The error in the directional response for 1000 W m^{-2} of direct beam irradiance is less than 10 W m^{-2} for CM11 and less than 20 W m^{-2} for CMP6 at all solar zenith and azimuth angles (Kipp & Zonen 2000, 2014; C. Lee (Kipp & Zonen) pers. comm.).

Due to the large field of view of the pyranometer, reflections from the surrounding non-deposited snow surface have an impact on the measurements of reflected global radiation above the deposited area. The albedo derived using the measurement set-up described herein essentially quantifies the magnitude of this disturbance in the albedo. Measurements over pure non-deposited snow represent the reference case, whereas measurements over deposited areas yield the cases of disturbance caused by deposition.

Elemental carbon measurements in snow

In the experiments, soot (which includes BC) was spread onto the snow surface, but actual BC concentrations were not measured. The definition of BC is operational: it is measured with

optical methods, where it is assumed that the light-absorbing substance is BC. However, in this study instead of BC the concentration of Elemental Carbon (EC) was measured. EC is also defined by the method; it is measured with thermal methods [for definitions *see* e.g. Andreae and Gelenscer (2006), and Bond *et al*. (2013)]. It has been observed in several studies that EC is the most efficient light-absorbing substance in aerosols so EC and BC are often considered to be equivalent even though there is a clear difference in their definitions.

Snow samples for EC analysis were collected in 5 by 5 cm increments from each spot after the soot had been deposited (within 12 hours of deposition). In addition to this sampling in SoS2013, snow samples were collected from two spots (S5 and S7) at a later stage, specifically nine days after soot deposition. The purpose of these measurements was to observe if the soot particles would remain in the surface snow or not. This temporal study was in spots where albedo measurements were not conducted.

Collected snow samples were analyzed for Organic Carbon (OC) and EC content using a Sunset Laboratory Thermal-Optical Carbon Aerosol Analyzer (OC/EC; Birch and Cary 1996) following the filter-based method used in e.g. Forsström *et al*. (2009, 2013) and Svensson *et al*. (2013). Briefly, the frozen snow samples were melted quickly in a microwave oven and filtered through a sterilized microquartz filter, which was then analyzed with OC/EC using the latest recommended analysis protocol EUSAAR_2 (Cavalli *et al*. 2010). The analysis yields the mass of EC on the filter. The concentration in snow is calculated by dividing the EC mass by the mass of snow in the sample, yielding concentrations which are typically presented as ng of EC in g of snow, i.e., ng g^{-1}, also known as parts per billion (ppb).

Uncertainties of the filter method are related to representativeness of the punch taken for the analysis (typically 1.5 cm^2 of the filter which has an area of ~10 cm^2), and the efficiency of the filter to capture all the EC particles from the liquid sample during filtering (also known as undercatch). Based on relative standard deviation of EC concentrations measured for different filter punches from the same filter, representativeness of the filter punch has been reported to be on the order of 20% (Svensson *et al*. 2013, Ruppel *et al*. 2014). This value is based on filters with a visible gradient of impurities. From our experience, however, filters tend to have impurities uniformly distributed on their surfaces (which was the case for the majority of the filters in our experiments), resulting in a much lower difference between punches (less than 5% as in Ruppel *et al*. 2014).

Undercatch is another uncertainty issue that has been shown to take place during filtering (Ogren *et al*. 1983, Lavanchy *et al*. 1999, Doherty *et al*. 2010, Forsström *et al*. 2013, Lim *et al*. 2014, Torres *et al*. 2014). The efficiency has been shown to be very inconsistent, ranging from 10% to 95%, among different studies and methods to evaluate the efficiency of filters. Filters have been stacked on top of each other or put in series (separated) to increase the efficiency of collecting EC (or BC with optical measurement methods) particles, both of which have recently been shown to be misleading in the actual efficiency of the filters, thus indicating a higher efficiency than there actually is (Torres *et al*. 2014). Additionally, liquid samples have been measured with a different instrument (single particle soot photometer, SP2) before and after filtration to observe the amount of particles percolating through the filter (Lim *et al*. 2014, Torres *et al*. 2014). It was shown that up to 90% of the BC particles could possibly penetrate through the filter (Torres *et al*. 2014), while, in contrast, Lim *et al*. (2014) found that as little as 10% of the BC particles could be passing through the filter. This discrepancy seems to depend on the origin of the liquid sample, and consequently the BC particles in it, as well as agglomeration processes occurring between BC particles and other light-absorbing impurities such as dust in the liquid. The majority of BC particles that are percolating through the filter during filtration seem to be smaller in size (Lim *et al*. 2014). In our experiments, the size distribution of the EC particles was shifted towards the larger sizes (as many larger particles were observed in the electron microscopy images). Therefore, we claim that we had a relatively high efficiency of our filters during filtering. Nonetheless, the EC concentrations from the experiments are probably an underestimation of the true EC concentration

in the snow samples. At this time, we are unfortunately not able to quantify the underestimation of EC, however, we consider it to be < 22%, based on Forsström *et al*. (2013).

Electron microscopic analyses

In addition to the OC/EC analysis, one snow sample containing soot particles from SoS2013 was analyzed using electron microscopy at the Chemistry Department of the University of Helsinki. The sample was taken immediately after depositing the snow and transported frozen to Helsinki. There it was melted over a smooth silicon plate and dried by letting the water evaporate inside an over-pressurized, clean hood to minimize the possibility of contamination. A small amount, of ethanol (< 10 ml) was added to the snow before it was melted in order to minimize agglomeration of particles during the melting and drying. The particles were studied with a Hitachi Hi-tech S-4800 field-emission electron microscope fitted with an Oxford Instruments Inca 350 energy-dispersive X-ray microanalysis (EDS) system. Soot particles were identified as such by EDS measurements with both 5 kV and 20 kV acceleration voltages. The 5 kV measurements were used for detecting carbon and oxygen in the soot particles, and the 20 kV measurements were used to check for metals present in mineral dust, such as Na, Al, Ca, Fe. While some mixed soot/mineral particles were found, particles without mineral content were mainly used for assessing particle sizes. Soot particle sizes were spread over three orders of magnitude, from 0.1 to 10 μm in size (Fig. 3). Particles larger than 5 μm were rare and particles smaller than 1.0 μm were the most numerous. The 0.1 to 1.0 μm particles were present both as individual particles and as larger microscale agglomerates.

Snow physical characteristics measurements

In SoS2011, two snow pits were dug (one in the clean reference site and the other in the snow with the soot) on 1 April, which was approximately one month after soot deposition. In the pits, the snow stratigraphy was measured, including thickness, density, hardness (6 step hand test), grain size, and the shape (following the International Classification for Seasonal Snow on the Ground, Fierz *et al*. 2009). The grain sizes and types were determined using an 8× magnifying glass and a millimeter-scale grid. The reported snow grain size is the greatest extension of a grain.

In SoS2013, the snow characteristics of the snowpack were recorded at a few different sites before the soot deposition. During melting, another set of observations were made at two spots (S5 and S7) and a reference area to record effects of the BC on the snow properties. The snow pits were dug in a similar manner as in SoS2011 with slight differences in the methodology of grain size determination. The snow layers were first defined based on visual and manual detection of density, hardness, and grain size differences. For each separate layer, the hardness index, wetness index, and snow grain type were defined following Fierz *et al*. (2009). Each snow pit had its temperature profile (every 10 cm) and a density profile (every 5 cm) recorded. For snow grain-size determination, a small sample of snow for each layer was macro-photographed against a 1 mm grid. From the photographs, the average, minimum, and maximum diameter of a 'typical' snow grain was then visually estimated to the closest 0.25 mm.

Results and discussion

Albedo

The time resolution of the raw albedo data was one minute, but here the temporal evolution of the albedo from the contaminated and clean snow is presented as 1-h averages at solar noon ± 30 minutes (Fig. 4). The temperature and the daily precipitation time series were also plotted for both experiments to help in the interpretation of albedo variations. Unfortunately, temperature and precipitation were not measured in the immediate vicinity of the experimental fields: the 2011 weather data originate from the FMI measurements at the Helsinki-Vantaa airport about 17 km east-southeast of the experiment, and the 2013 data from the FMI Sodankylä observatory about 3.5 km south of the site.

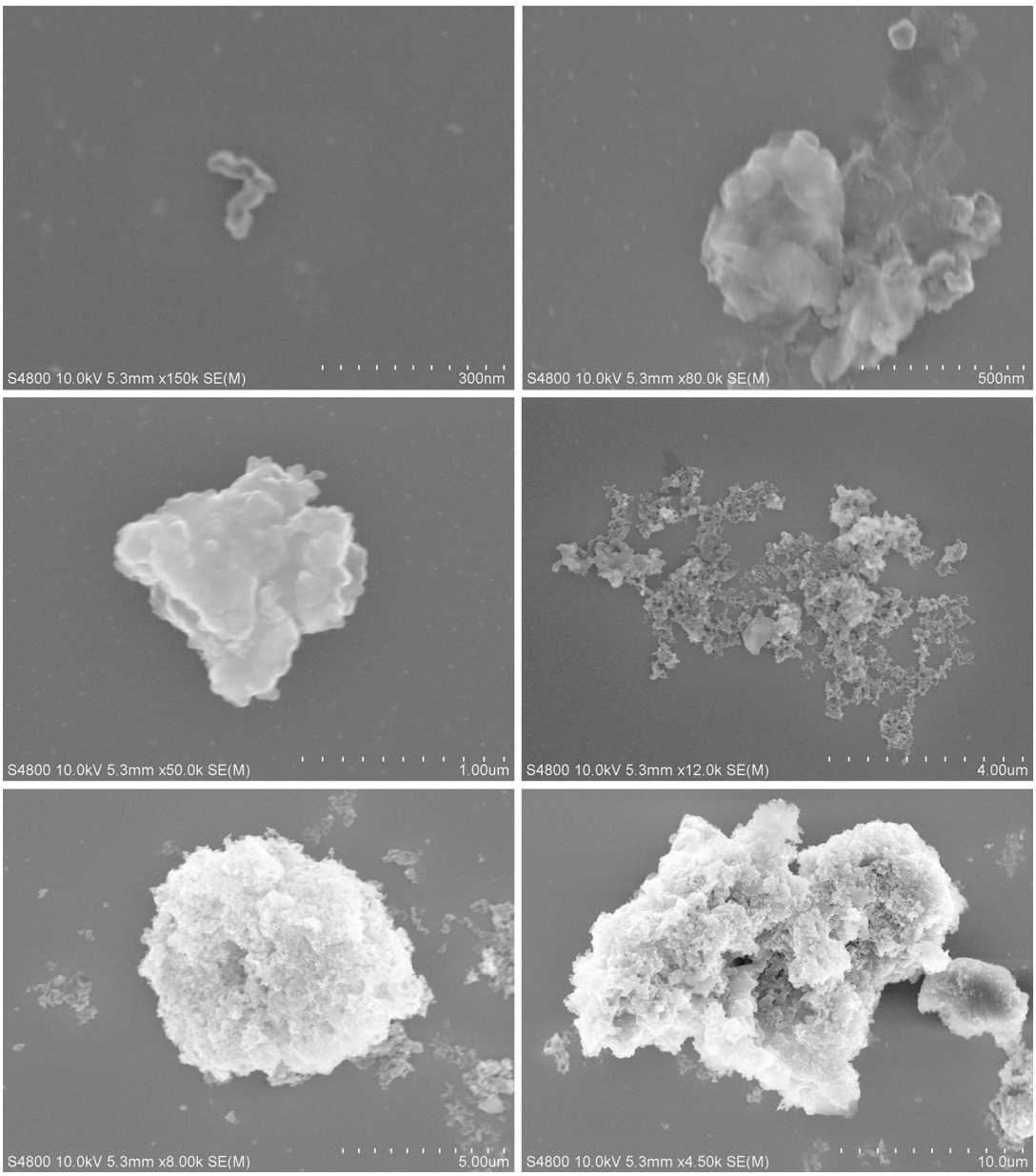

Fig. 3. SEM images of soot particles of various sizes originating from chimney sweeping of wood-burning residential homes, deposited onto spot 1 in SoS2013.

SoS2011

After the soot deposition, the snow-surface albedo dropped to 0.52, while the albedo of the reference snow was 0.83 (Fig. 4a). At this time, the average corresponding EC concentrations of the soot-doped-snow and clean-snow surfaces were 20 900 ng g^{-1} and 80 ng g^{-1}, respectively (Table 2). The albedo of the soot-covered snow decreased the next day to 0.39, after which it increased for two days, and thereafter reached a minimum value of 0.35 on 10 March. During the same period, the reference-snow albedo increased to 0.86 on the second day of measurements, and thereafter had some small fluctuations until it reached 0.80 on 10 March. A pos-

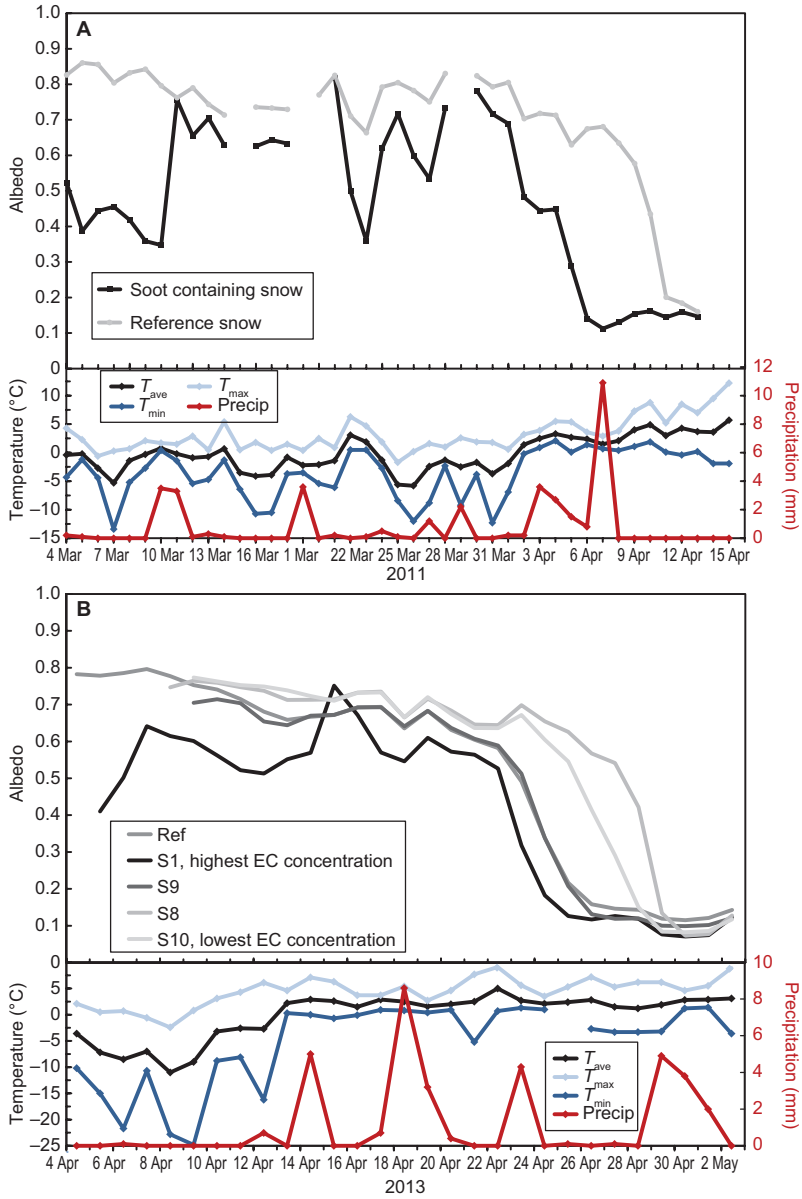

Fig. 4. Albedo time series and meteorological conditions during the experiments: (**A**) SoS2011 and (**B**) SoS2013.

sible explanation for the rapid decrease of the soot-containing-snow albedo is that the daytime temperatures were often close to or above zero, which would imply heating of snow and grain size growth. With larger snow grains the albedo-reducing effect of soot is further increased (Warren and Wiscombe 1980, Hadley and Kirchstetter 2012).

Snowfall on 10 and 11 March resulted in an increase of the albedo of the sooted snow to 0.76, while that of the reference decreased to 0.76 during the same time. Our hypothesis is that the newly-fallen snow had an albedo of 0.76, which was observed in both of the snow patches. Following this event, the albedo of the sooted snow decreased somewhat and remained in the range of 0.7–0.6 for the following week, while the albedo of the reference snow was about 10% higher at that time. Another major snowfall event on 19 March covered the pyranometers, resulting in the data gap on 19–20 March. During this event, the snow accumulated

onto the upward-looking sensor preventing the instrument from proper collection of photons, resulting in the irradiance values close to zero, and consequently albedo values exceeding unity. After cleaning the pyranometers on 21 March the albedo increased to 0.82 and 0.83 for the sooted and the reference snow, respectively. During the subsequent two days, a rapid decrease in the albedo of the sooted snow occurred, while that of the reference snow did not decease to the same degree. A possible explanation for the decrease of the sooted snow albedo is that the soot below the fresh snow absorbed solar radiation which increased melting of the new snow. This also led to a higher temperature and again morphological changes in the fresh snow above the soot layer. The rapid decrease in albedo during this period was enhanced by the meteorological conditions, as the temperature reached above 0 °C (for both average and minimum), which promotes snow grain growth and an ensuing decrease in albedo.

Similar events, with new snow, occurred later with the albedo fluctuating until 2 April, when snowmelt started and the albedo steadily decreasing until the snowpack was completely gone on 6 April. This was not the case for the reference snow as the albedo remained in the range of 0.81–0.68 between 1 and 7 April. The rapid decrease started after this date and on 11 April the albedo was down to 0.2, with the entire snowpack melted at that time.

SoS2013

After soot deposition, the albedo was the lowest at the spots with the highest amount of soot and vice versa, the albedo was the highest at the spots with the lowest amount of soot (*see* Table 2 for EC concentrations of the different spots). There were differences and similarities in the albedo time series of SoS2013 and SoS2011. Probably the most obvious difference was at the beginning of the experiment. The albedo time series (Fig. 4B) shows a sharp increase of 0.23 in the albedo of the most contaminated spot during the first two measurements days of SoS2013, just opposite to the decreasing albedo of the dark spot of SoS2011. This increase in SoS2013 could be explained by the fact that after deposition, the soot particles sunk into the snow surface, within minutes of deposition, as visually observed and further described in Peltoniemi *et al*. (2015). The soot particles sunk during the day at elevated solar radiation, and thereafter stopped sinking during the nights when the temperature was well below zero (indicated by the temperature minimum in Fig. 4b). There was a minor snowfall on 6 April which may have contributed to the increase in albedo as well. The albedo started to decrease again on the third day of measurements for the most contaminated spot. On 14 April, a snow shower put few centimeters of fresh snow on the snowpack. A distinct increase in the albedo was observed between 14 and 15 April for the most contaminated spot. This increase was not as pronounced for the other spots. Similar to the snowfall events in SoS2011, the melting of the fresh snow and decrease in albedo occurred fastest on the spot where the soot concentration was highest. It was also around this time (14 April 2013) that the melting accelerated as the average temperature remained above 0 °C for the remaining part of the experiment. The snow depth was approximately 50 cm on 15 April, while on 17 April it had decreased to roughly 35 cm. Another event with an increase in the albedo, visible in all spots, occurred on 18 and 19 April. During this time the pyranometer sensors were all lowered by 20 cm, which could potentially explain the albedo increase.

On 22 April, the albedo began to decrease rapidly starting with the spot with the highest BC concentration changing its albedo from 0.55 to 0.15 during 72 hours. The spots with lower BC concentrations followed this rapid decrease in albedo a few days later. The temporal variation of the albedo at Spot S9 (second highest EC concentration) and the contaminated reference spot (named Ref in Fig. 4B) were nearly identical during this fast albedo reduction. The albedo decreased earlier at the spot with the lowest EC concentration (S10) than at the spot with the second lowest EC concentration (S8). However, since at this time snow samples were not collected for determination of the EC concentrations for these spots, those concentrations are unknown. Further, it is unclear to what extent BC affected snowmelt (especially with lower EC concentrations) when the snowpack height was

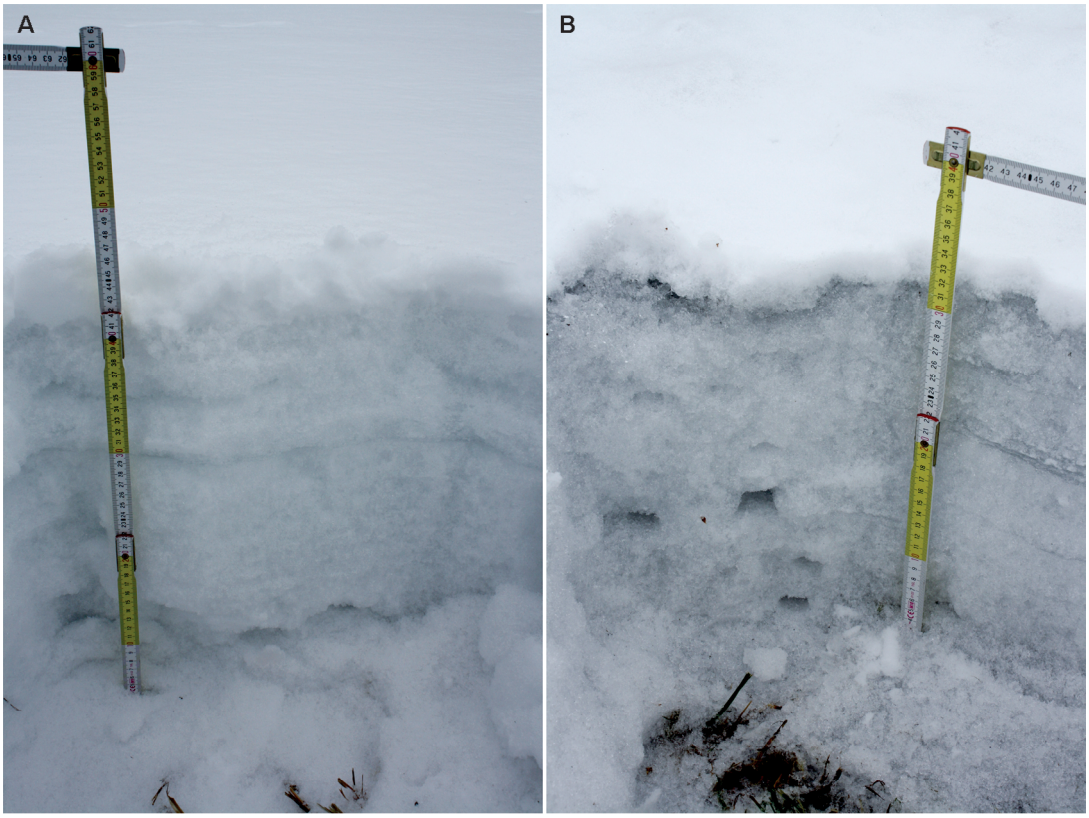

Fig. 5. Snow pits from SoS2011. (**A**) Reference snow about one month after deposition of the soot onto the snow in SoS2011, and (**B**) Soot-contaminated snow at the same time.

smaller than ~30 cm, when one would expect the albedo of the underlying ground to have a significant effect on snow melt.

Physical snow characteristics

In SoS2011, the melting rates of the snow at the reference site and at the soot-contaminated spot were 3 cm and 7 cm per day, respectively. From the snow pits dug and studied one month after soot deposition in SoS2011, it was evident that the snow containing the soot had changed more than the reference snow (Appendixes 1 and 2, Fig. 5). Although, no snow-pit measurements were performed before soot deposition it is very likely that those changes were due to the deposited soot since the snow pits were only 15 m apart on a homogenous farming field and the EC concentrations were high. As no other snow pits were dug, it cannot, however, be considered proven. The soot-doped snow had transformed to a more homogenous snowpack containing rounded polycrystal snow grains, whereas the grain shapes of the reference snow were more heterogeneous. Similarly, the hardness test revealed a more uniform pattern in the sooted snow, while the reference site was more diverse. The snow depth for the dirty snowpack was at that time 35 cm, while the clean snow had a depth of 50 cm. Both of the pits had a layer of freshly fallen snow (4-cm deep at the reference site and 2-cm deep at the sooted snow), containing 0.5-mm snow grains. The grain size of the remaining snow was 2 mm, except for the bottom 5 cm at the reference site, where it was 1 mm. The snow density for the two snow pits was practically the same. It varied between 340 and 400 kg m^{-3} in the top part of the snowpack and was 460 kg m^{-3} at the bottom. Since the snowpack had brittle layers and also some very loose layers, it was difficult to conduct the

density measurements and therefore only few density data were obtained.

Before the soot deposition in SoS2013, the density in the surface layer varied between 0.208 and 0.290 g cm^{-3}, with an average of 0.247 g cm^{-3} for the three pits measured before applying the soot to the snow (Appendixes 3–7). Irregular precipitation particles were visible in the top centimeters of those pits, after which rounded faceted crystals were present before the depth hoar grains in the bottom of the snowpack. The average visual grain sizes in the top layer was 0.25 mm and 0.5 mm, followed by 0.75 mm and 1 mm in the subsequent layer (grain size measurements were conducted for two out of the three pits sampled before soot deposition). By 10 April 2013, snow-pit measurements in two of the sooted spots (S5 and S7) revealed that the precipitation particles in the surface layers had melted and a hard melt-freeze layer had developed near the snow surface (Appendixes 8–11). The average surface grain sizes at these spots were estimated to be 0.5 mm and 1 mm, respectively. In addition, larger aggregates produced by snow grains melting and refreezing together were found near the surface. Snow-pit measurements made two days earlier in the nearby mire and forested areas, revealed the same kind of snow stratification, which would indicate that the melt-freeze layers were not only produced by the presence of light absorbing impurities but were caused by the changes in the weather conditions as well. It is, however, hypothesized that the impurities may enhance the development of surface crusts by enhancing the snow melt during the sunny hours, while the air temperature still drops below zero at nighttime. The snow characteristics of spots S5 and S7 plus a clean reference snow were measured again on 17 April 2013. At that time, snowmelt had already started with the temperature of the whole snowpack being 0 °C, and snow grain types of rounded melt forms were recorded (Appendixes 12–17). The average surface grain size in all three spots was estimated to be 1 mm.

During SoS2013, we observed that the soot containing snow lowered the density of melting snow (Meinander *et al*. 2014). We also observed that light-absorbing impurities deposited on the snow enhance the immediate metamorphosis under strong sunlight (Peltoniemi *et al*. 2015). After soot deposition, the contaminated snow surface was darker than the pure snow in all viewing directions, but as stated above, we observed the soot particles sinking into the snow, thus increasing its surface roughness.

Elemental carbon in SoS2013 surface snow

For the two spots (S5 and S7) which were used for the temporal study of the soot particles, we calculated the EC mass concentrations in the surface layers, by multiplying the EC concentration in the surface layer with the surface density of the snow, and also by subtracting the background EC mass concentration in the reference snow surface layer (Appendix 7). Since the density of the surface layer was not measured in S7, the average density from all snow surface layer (0–5 cm) measurements before soot deposition was used in these calculations.

The EC mass concentrations on 10 April could thereafter be compared with the EC mass concentrations from surface samples collected on 17 April, and thus provide a fraction of the EC particles which had remained in the surface layer during this time while melting had occurred.

On 10 April, the EC mass concentration was 374 ng cm^{-3} for S5 (Appendix 9) and 323 ng cm^{-3} (Appendix 11) for S7. After the seven day period, the EC mass concentration was 233 ng cm^{-3} for S5 (Appendix 15), while in the surface layer of S7 then EC mass concentration was 154 ng cm^{-3} (Appendix 17). In other words, 48% of the EC particles had remained in the surface layer during this period in S7, while 62% of the EC particles remained in S5. Using a lower background EC mass concentration, from a snow sample collected a few kilometers away from the FMI observatory and which had not been at risk of contamination, we calculated that 56% of the EC particles remained at the surface in S7, while the number was 70% for S5, hence providing upper estimates for the amount of particles remaining in the surface snow during melt.

Based on our values, about half of the initial soot which had been deposited to the snow sur-

face had been removed. In Conway *et al*. (1996), where hydrophobic and hydrophilic soot was also investigated to observe movement of the soot particles, about 50% of the initial hydrophobic soot had been flushed through the snowpack after 10 days, while the hydrophilic soot had 1% of the initial soot remained in the upper 50 cm of the snowpack. In comparison, ambient measurements have shown that confined to the top centimeters of the snowpack, the BC concentrations in the snow during the melt have been found to increase by a factor of 2–7 (Doherty *et al*. 2013, Sterle *et al*. 2013). Doherty *et al*. (2013) found an even higher amplification factor of ~10–15, when the melting-snow BC concentrations were compared with the concentrations measured earlier in the year at a site near Dye-2, on the Greenland ice sheet.

Parameterization and comparison with previous works

The albedo measured during the first three days of the SoS experiments was plotted against the EC concentration, [EC] (Fig. 6). Fitting was done using the following function:

$$\text{albedo} = b \times [\text{EC}]^c + d, \qquad (1)$$

where b, c and d are the fitting parameters. Different fittings were made by excluding and including the most contaminated spot from SoS2011, for individual days 1, 2 and 3, as well as for the all three days together (Table 3). In all fittings the highest albedo was that of the reference spot in SoS2011, 0.83 ± 0.02 (based on the 1-week average). A similar function was also used in a recent BC snow-modeling effort by Hienola *et al*. (2015).

Data from Hadley and Kirchstetter (2012) and Pedersen *et al*. (2015) are also presented in Fig. 6 for comparison. The work of Pedersen *et al*. (2015) was based on measurements of EC concentrations and the corresponding spectral albedo of the snow. They parameterized their spectral data essentially with the same function as ours (Eq. 1) but presented the resulting curve for the broadband albedo only in a figure (Pedersen *et al*. 2015: fig. 8). We digitized their fig. 8, fitted the function (Eq. 1), and obtained b = 0.001049 and c = 0.6334 for cloudy conditions, and b = 0.0009190 and c = 0.6332 for clear-sky conditions that describe the dependence on EC concentration. The corresponding lines were then forced to go through our reference albedo *versus* EC point to get the factor d in Eq. 1 (Fig. 6). It is evident that our experimental data agree quite well with those of Pedersen *et al*. (2015).

The behavior of albedo with EC concentration in the SoS experiments also seems to generally follow that observed in the laboratory study by Hadley and Kirchstetter (2012). It especially applies for the two lower snow grain sizes used in their experiments (110 and 130 μm), while their grain size of 220 μm showed a greater albedo reduction with similar EC concentrations (Fig. 6). Thus, our experiments show how the effects of BC on natural snow in outdoor conditions are not as pronounced as those in the laboratory conditions used in Hadley and Kirchstetter (2012). Since their laboratory study applies to a solar zenith angle of 0°, when the albedo reduction due to BC is the strongest, it is in agreement with our outdoor light conditions, where the solar zenith angle is different.

Table 3. Parameters *b*, *c* and *d* obtained by fitting Eq. 1 to the observations. ExclDS11 = fitting excluding the dark spot in 2011, and InclDS11 = fitting including the dark spot in 2011.

	Day 1		Day 2		Day 3		Days 1–3	
	ExclDS	InclDS11	ExclDS11	InclDS11	ExclDS11	InclDS11	ExclDS11	InclDS11
b	–0.140	–2.557	–0.127	–0.257	–0.425	–0.085	–0.150	–0.358
c	0.617	0.028	0.545	0.275	0.100	0.489	0.455	0.185
d	0.851	3.238	0.851	0.965	1.152	0.827	0.868	1.062

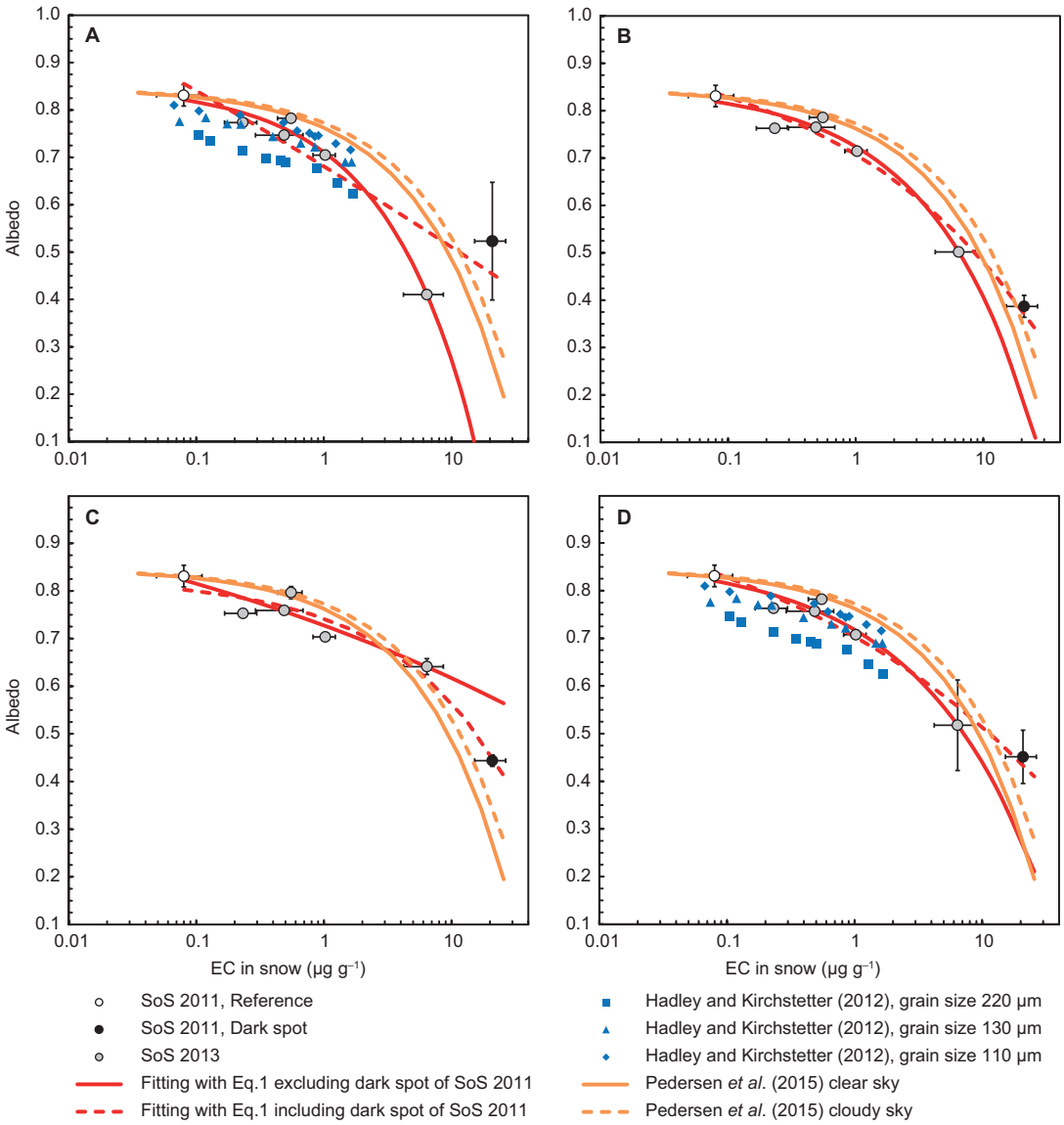

Fig. 6. Broadband albedos at noon on days 1–3 as a function of the EC concentration in the surface layer: (**A**) day 1, (**B**) day 2, (B) day 3, and (**D**) days 1–3. In all plots, the SoS2011 reference albedo is the average over solar noon albedos during the first week of the experiment. In **A–C,** the gray and black circles are 60-minute albedo averages at solar noon, the vertical and horizontal bars are standard deviations for albedo and EC, respectively. In **D,** the circles are the albedo averages at solar noon of the days 1–3, and the vertical and horizontal bars are standard deviations for albedo and EC, respectively.

Conclusions and recommendations for the future

In our soot on snow experiments it was found that BC has an effect on the broadband albedo of natural snow. This has been verified in controlled, laboratory studies and with artificial snowpacks, but to our knowledge no such results have been published from field experiments using natural snow and dry deposition of soot. With higher amounts of soot we observed a greater reduction in snow albedo than with lower soot concentrations. It was further observed that the BC effect on snow may be masked by

deposition of new snow, burying the original soot layer in the snowpack. Melting of the newly-added snow progressed faster for the snow patch containing the buried soot layer, however, than for the reference snow where no impurities were added.

With the approach used in our experiments certain challenges were present. For example, at low soot concentrations it would be difficult to observe the BC effect clearly since snow albedo depends on many other parameters, particularly snow grain size. In parts-per-billion concentrations of soot (on the order of 10's) in the snow, which has been reported in the Arctic snowpack (e.g. Doherty *et al*. 2010), the albedo reduction caused by the BC is so small that any measured albedo reduction could be caused by the uncertainties introduced when carrying out an experiment of this nature. Performing the experiments outdoors brought additional natural challenges such as non-ideal meteorological conditions as well as different solar circumstances, which cannot be reproduced in laboratory facilities. Nevertheless, our goal was to conduct these experiments since it had not been done before. BC in snow still requires experimental studies in order to better constrain the BC forcing on snow and to improve the process understanding associated with BC in the snow.

The soot particles did not all remain on the snow surface with time. About half of the initial soot amount was in the surface layer after seven days of melting. These numbers can be considered qualitative since several uncertainties exist. Additional experiments are needed to deliver sound quantitative numbers on this topic.

The experience gained during the three SoS experiments leads to the following recommendations for future studies:

1. To avoid surface effects on the melting rate, experimental spots should be located where the underlying surface albedo is spatially homogeneous and preferably high.
2. As it is difficult to deposit soot onto the snow in a controlled way with the two methods used here, a development of different blowing system should be considered.
3. The measurements should be commenced immediately after soot deposition. It was observed that within minutes the soot start to interact with the snow crystals (especially during sunny days), as the particles sunk into the snow immediately following deposition.
4. More detailed observations of the physical snow properties are needed to study the temporal dynamics of BC in the snowpack, and to more accurately provide quantitative numbers on the process of BC sticking at the snow surface.
5. Broadband albedo measurements should be compared with the spectral albedo measurements of soot-contaminated snow to better constrain the BC effect on snow albedo.

Acknowledgements: We would like to thank Antti Aarva for helping us with numerous issues throughout these experiments. The work of the technical staff at FMI, Sodankylä, during SoS2013 is very much appreciated. The Chimney sweeping company (Consti Talotekniikka Oy) is acknowledged for supplying us with the soot. The authors wish to acknowledge Mr. Markku Sinkkonen at Vaisala Oyj and Mr. Clive Lee at Kipp & Zonen for providing the information needed for the compilation of the uncertainty budgets for the pyranometers. Mr. Timo Vainio is acknowledged for the use of his farming field in SoS2011 and Mrs. Anita Virkkula for preparing the experimental chamber. We would also like to thanks Odelle Hadley and Thomas Kirchstetter for sharing their data. This work has been supported by the Academy of Finland through the projects: Arctic Absorbing Aerosols and Albedo of Snow (project no. 3162), and the Electromagnetic Wave Scattering in a Complex Random Medium (project no. 260027). This work has also been supported by the EU LIFE+ project MACEB (project no. LIFE09 ENV/FI/000572the European Commission ERC Advanced Grant No. 320773 (SAEMPL); the Maj and Tor Nessling Foundation (projects 2012456 and 2013093); the KONE foundation; and the Nordic research and innovation initiative Cryosphere-Atmosphere Interactions in a Changing Arctic Climate (CRAICC). Research at the Ural Federal University is supported by the Act 211 of the Government of the Russian Federation, Agreement No. 02.A03.21.0006.

References

Andreae M.O. & Gelencsér A. 2006. Black carbon or brown carbon? The nature of light-absorbing carbonaceous aerosols. *Atmos. Chem. Phys.* 6: 3131–3148.

Birch M.E. & Cary R.A. 1996. Elemental carbon-based method for monitoring occupational exposures to particulate diesel exhaust. *Aerosol. Sci. Tech.* 25: 221–241.

Bond T.C., Doherty S.J., Fahey D.W., Forster P.M., Berntsen T., DeAngelo B.J., Flanner M.G, Ghan S., Kärcher B., Koch D., Kinne S., Kondo Y., Quinn P.K., Sarofim M.F., Schultz M.G., Schulz M., Venkataraman C., Zhang H.,

Zhang S., Bellouin N., Guttikunda S.K., Hopke P.K., Jacobson M.Z., Kaiser J.W., Klimont Z., Lohmann U., Schwarz J.P., Shindell D., Storelvmo T., Warren S.G. & Zender C.S. 2013. Bounding the role of black carbon in the climate system: a scientific assessment. *J. Geophys. Res.* 188: 5380–5552.

Brandt R.E., Warren S.G. & Clarke A.D. 2011. A controlled snowmaking experiment testing the relation between black-carbon content and reduction of snow albedo. *J. Geophys. Res.* 116, D08109, doi:10.1029/2010JD01533.

Cavalli F., Viana M., Yttri K.E., Genberg J. & Putaud J.-P. 2010. Toward a standardised thermal-optical protocol for measuring atmospheric organic and elemental carbon: the EUSAAR protocol. *Atmos. Meas. Tech.* 3: 79–89.

Clarke A.D. & Noone K.J. 1985. Soot in the Arctic snowpack: a cause for perturbations in radiative transfer. *Atmos. Environ.* 19: 2045–2053.

Conway H., Gades A. & Raymond C.F. 1996. Albedo of dirty snow during conditions of melt. *Water Resour. Res.* 32: 1713–1718.

Doherty S.J., Warren S.G., Grenfell T.C., Clarke A.D. & Brandt R.E. 2010. Light-absorbing impurities in Arctic snow. *Atmos. Chem. Phys.* 10: 11647–11680.

Doherty S.J., Grenfell T.C., Forsstrom S., Hegg D.L., Brandt R.E. & Warren S.G. 2013. Observed vertical redistribution of black carbon and other insoluble light-absorbing particles in melting snow. *J. Geophys. Res.* 118: 1–17.

Fierz C., Armstrong R.L., Durand Y., Etchevers P., Greene E., McClung D.M., Nishimura K., Satyawali P.K. & Sokratov S.A. 2009. *The international classification for seasonal snow on the ground*. IHP-VII Technical Documents in Hydrology no. 83, IACS Contribution no. 1, UNESCO-IHP, Paris.

Fily M., Bourdelles B., Dedieu J.P. & Sergent C. 1997. Comparison of in situ and Landsat Thematic Mapper derived snow grain characteristics in the Alps. *Remote Sens. Environ.* 59: 452–460.

Flanner M.G., Zender C.S., Randerson J.T. & Rasch P.J. 2007. Present-day climate forcing and response from black carbon in snow. *J. Geophys. Res.* 112, D11202, doi:10.1029/2006JD008003.

Forsström S., Ström J., Pedersen C.A., Isaksson E & Gerland S. 2009. Elemental carbon distribution in Svalbard snow. *J. Geophys. Res.* 114, D19112, doi:10.1029/2008JD011480.

Forsström S., Isaksson E., Skeie R.B., Ström J., Pedersen C.A., Hudson S.R., Berntsen T.K., Lihavainen H., Godtliebsen F. & Gerland S. 2013. Elemental carbon measurements in European Arctic snow packs. *J. Geophys. Res.* 118: 13614–13627.

Hadley O.L. & Kirchstetter T.W. 2012. Black-carbon reduction of snow albedo. *Nat. Clim. Change* 2: 437–440.

Hienola A.I., O'Donnell D., Pietkäinen J-K., Svensson J., Lihavainen H., Virkkula A., Korhonen H. & Laaksonen A. 2015. The radiative impact of Nordic anthropogenic black carbon. *Tellus* 68, 27428, doi:/10.3402/tellusb.v68.27428.

ISO9060:1990 1990. *Solar energy — specification and classification of instruments for measuring hemispherical solar and direct solar radiation*. International Organization for Standardization.

JCGM 2008. *Guide to the expression of uncertainty in measurement (ISO/IEC Guide 98-3:2008), ISO GUM 1995 with minor corrections*, 1st ed. Available at http://www.iso.org/sites/JCGM/GUM/JCGM100/C045315e-html/C045315e.html?csnumber=50461.

Kaspari S., Painter T.H., Gysel M., Skiles S.M. & Schwikowski M. 2014. Seasonal and elevational variations of black carbon and dust in snow and ice in the Solu-Khumbu, Nepal and estimated radiative forcings. *Atmos. Chem. Phys.* 14: 8089–8103.

Kipp & Zonen 2000. *Instruction manual CM11 & CM14 Series Pyranometer/Albedometer*, ver. 1104. Kipp & Zonen, Delft, Holland.

Kipp & Zonen 2014. *Instruction manual CMP & CMA Series Pyranometer/Albedometer*, ver. 1401. Kipp & Zonen, Delft, Holland.

Kratzenberg M., Beyer H., Colle S. & Albertazzi A. 2006. Uncertainty calculations in pyranometer measurements and application. In: *ASME 2006 International Solar Energy Conference (ISEC2006), July 8–13, Denver, Colorado, U.S.A.*, American Society of Mechanical Engineers, paper ISEC2006-99168, pp. 689–698, doi:10.1115/ISEC2006-99168.

Lavanchy V.M.H., Gäggler H.W., Schotterer U., Schwikowski M. & Baltensperger U. 1999. Historical record of carbonaceous particle concentrations from a European high-alpine glacier (Colle Gnifetti, Switzerland). *J. Geophys. Res.* 104: 21227–21236.

Lim S., Faïn X., Zanatta M., Cozic J., Jaffrezo J.-L., Ginot P. & Laj P. 2014. Refractory black carbon mass concentrations in snow and ice: method evaluation and inter-comparison with elemental carbon measurement. *Atmos. Meas. Tech.* 7: 3307–3324.

Meinander O., Kontu A., Virkkula A., Arola A., Backman L., Dagsson-Waldhauserová P., Järvinen O., Manninen T., Svensson J., de Leeuw G. & Leppäranta M. 2014. Brief communication: Light-absorbing impurities can reduce the density of melting snow. *The Cryosphere* 8: 991–995.

Meinander O., Kazadzis S., Arola A., Riihelä A., Räisänen P., Kivi R., Kontu A., Kouznetsov R., Sofiev M., Svensson J., Suokanerva H., Aaltonen V., Manninen T., Roujean J.-L. & Hautecoeur O. 2013. Spectral albedo of seasonal snow during intensive melt period at Sodankylä, beyond the Arctic Circle. *Atmos. Chem. Phys.* 13: 3793–3810.

Ogren J.A., Charlson R.J. & Grobllckl P.J. 1983. Determination of elemental carbon in rainwater. *Anal. Chem.* 55: 1569–1572.

Pedersen C.A., Gallet J.-C., Ström J., Gerland S., Hudson S.R., Forsström S., Isaksson E. & Berntsen T.K. 2015. In situ observations of black carbon in snow and the corresponding spectral surface albedo reduction. *J. Geophys. Res.* 120: 1476–1489.

Peltoniemi J.I., Gritsevich M., Hakala T., Dagsson-Waldhauserová P., Arnalds Ó., Anttila K., Hannula H.-R., Kivekäs N., Lihavainen H., Meinander O., Svensson J., Virkkula A. & de Leeuw G. 2015. Soot on Snow experiment: bidirectional reflectance factor measurements of contaminated snow. *The Cryosphere* 9: 2323–2337.

Qu B., Ming J., Kang S.-C., Zhang G.-S., Li Y.-W., Li C.-D.,

Zhao S.-Y., Ji Z.-M. & Cao J.-J. 2014. The decreasing albedo of the Zhadang glacier on western Nyainqentanglha and the role of light-absorbing impurities. *Atmos. Chem. Phys.* 14: 11117–11128.

Rypdal K., Rive N., Berntsen T.K., Klimont Z., Mideksa T.K., Myhre G. & Skeie R.B. 2009. Costs and global impacts of black carbon abatement strategies. *Tellus* 61B: 625–641.

Ruppel M.M., Isaksson E., Ström J., Beaudon E., Svensson J., Pedersen C.A. & Korhola A. 2014. Increase in elemental carbon values between 1970 and 2004 observed in a 300-year ice core from Holtedahlfonna (Svalbard). *Atmos. Chem. Phys.* 14: 11447–11469.

Skeie R.B., Berntsen T.K., Myhre G., Pedersen C.A., Ström J., Gerland S. & Ogren J.A. 2011. Black carbon in the atmosphere and snow, from pre-industrial times until present. *Atmos. Chem. Phys.* 11: 6809–6836.

Sterle K.M., McConnell J.R., Dozier J., Edwards R. & Flanner M.G. 2013. Retention and radiative forcing of black carbon in eastern Sierra Nevada snow. *The Croysphere* 7: 365–374.

Svensson J. Ström J., Hansson M., Lihavainen H. & Kerminen V.-M. 2013. Observed metre scale horizontal variability of elemental carbon in surface snow. *Environ. Res. Lett.* 8, 034012, doi:10.1088/1748-9326/8/3/034012.

Torres A., Bond T.C., Lehmann C.M.B., Subramanian R. & Hadley O.L. 2014. Measuring organic carbon and black carbon in rainwater: evaluation of methods. *Aerosol Sci. Technol.* 48: 239–250.

Warren S.G. & Wiscombe W.J. 1980. A model for the spectral albedo of snow. II: Snow containing atmospheric aerosols. *J. Atmos. Sci.* 37: 2734–2745.

WMO 2012: *Guide to meteorological instruments and methods of observation*, edition 2008 updated in 2010. WMO no. 8, Secretariat of the World Meteorological Organization, Geneva, Switzerland.

Xu B., Cao J., Joswiak D.R., Liu X., Zhao H. & He J. 2012. Post-depositional enrichment of black soot in snowpack and accelerated melting of Tibetan glaciers. *Environ. Res. Lett.* 7, 014022, doi:10.1088/1748-9326/7/1/014022.

Appendix 1. Reference snow stratigraphy about one month after soot deposition in SoS2011. Snow depth from the snow surface and the remaining parameters following Fierz *et al.* (2009).

Depth (cm)	Grain shape	Morphological classification subclass shape	Hardness	Size (mm)
0–4	RGlr	rounded	2	0.5–0.7
4–9	FCsf	faceted and some cup shaped	3	2
9–15	MFpc	rounded polycrystals	4	2
15–16		refrozen layer, rounded crystals	5	
16–45	FCxr	rounded by melting, some facted still left	3	2
45–50	MFpc	rounded polycrystals	4	1

Appendix 2. Soot contaminated snow stratigraphy about one month after soot deposition in SoS2011. Snow depth from the snow surface and the remaining parameters following Fierz *et al.* (2009).

Depth (cm)	Grain shape	Morphological classification subclass shape	Hardness	Size (mm)
0–2	RGlr	rounded	2	0.5
2–5	MFpc	rounded polycrystals	3	2
5–35	MFpc	rounded polycrystals	4	2

Appendix 3. Reference snow pit measured on 3 April 2013, in SoS2013.

Depth (cm)	Grain shape	Size	Hardness	Wetness	Grain size (mm)		
					Min	Max	Mean
0–3	Ppir	fine	1	2	0	1	0.25
3–16	RGxf	coarse	1	1	0.5	1.5	0.75
16–20	RGxf	coarse	1	1	0.25	1.75	1
20–31	Fcso	coarse/very coarse	1	1	0.5	2.5	1
31–39	FCso	coarse	2	1	0.5	2.25	1.25
39–52	DHcp + DHch	very coarse	1	1	0.5	4	1.5
52–66	DHcp	very coarse	4	1	0.75	4.25	2.25

Appendix 4. Reference snow pit measured on 3 April 2013, in SoS2013; n/a = not available.

Temperature		Density	
Depth (cm)	°C	Depth (cm)	g cm^{-3}
air	1.1	0–5	0.244
6	–6.6	5–10	0.272
16	–6.3	10–15	0.256
26	–5	15–20	0.248
36	–4.4	20–25	0.256
46	–3.8	25–30	0.300
56	–3.5	30–35	0.300
66	–3.2	35–40	0.244
		40–45	0.292
		45–50	0.324
		50–55	0.232
		55–60	n/a

Appendix 5. Reference snow pit measured on 5 April 2013, in SoS2013.

Depth (cm)	Grain shape	Density		Comments
		Depth (cm)	g cm^{-3}	
0–0.5	PPir	0–5	0.290	small crystalline, not dendritic
0.5–1.5	RGxf	5–10	0.360	more icy, more granular
1.5–4	FCsf	10–15	0.280	even more icy, grains larger
4–12.5	FCsf	15–20	0.240	similar as above
12.5–15	FCco	20–25	0.240	ice lens below harder
15–19	MFcf	25–30	0.300	rough icy grains
19–29	FCso	30–35	0.300	larger icy grains
29–32	FCso	35–40	0.250	below harder
32–42	FCso + DHcp	40–45	0.280	larger icy grains
42–47	DHcp + DHch	45–50	0.280	larger faceted icy grains
47–59	DHcp + DHch	50–55	0.250	larger icy grains, planar
59–64	DHcp + DHch	55–60	0.240	icy deep hoar
		59–64	0.220	

Appendix 6. Reference snow pit measured on 6 April 2013, in SoS2013.

Depth (cm)	Grain shape	Size	Hardness	Wetness	Grain size (mm)		
					Min	Max	Mean
0–1	Ppir	medium	1	1	0.25	0.75	0.50
1–9	RGxf	coarse	1	1	0.25	1.50	1.00
9–10	FCxr	coarse	1	1	0.50	2.50	1.00
10–16	FCxr	coarse	1	1	0.25	1.75	1.00
16–22	FCso	coarse	2	1	0.75	3.25	1.50
22–32	FCso	coarse	1	1	0.75	3.00	2.00
32–40	FCso	coarse	3	1	0.50	2.50	1.25
40–53	DHcp + DHch	very coarse	1	1	1.00	4.00	2.50
53–65	DHcp	very coarse	5	1	1.00	5.00	2.75

Appendix 7. Reference snow pit measured on 6 April 2013, in SoS2013; n/a = not available.

Temperature		Density		EC		
Depth (cm)	°C	Depth (cm)	g cm^{-3}	Depth (cm)	ng g^{-1}	ng cm^{-3}
air	–7.0	0–5	0.208	0–5	45.8	10.4
0	–10.0	5–10	0.224			
5	–11.8	10–15	0.248			
15	–8.9	15–20	0.320			
25	–5.8	20–25	0.252			
35	–4.7	25–30	0.244			
45	–3.7	30–35	0.296			
55	–3.2	35–40	0.280			
65	–2.8	40–45	0.260			
		45–50	0.272			
		50–55	0.280			
		55–60	0.320			
		60–65	n/a			

Appendix 8. Snow stratigraphy of S5, sampled on 10 April 2013, in SoS2013.

Depth (cm)	Grain shape	Size	Hardness	Wetness	Grain size (mm)		
					Min	Max	Mean
0–1	MFcr	very fine-very coarse	4	2	0.25	1.50	0.50
1–3	FCsf	coarse	1	1	0.75	2.00	1.25
3–13	FCxr	coarse	1	1	0.75	2.00	1.25
13–16	MFcr	medium	3	1	0.50	2.00	0.75
16–21	RG	coarse	3	1	0.75	1.50	1.00
21–28	FC/DH	very coarse	1	1	0.75	3.00	1.50
28–30	MFpc/MFcr	coarse	4	1	0.75	3.00	1.00
30–36	RGlr	coarse	4	1	0.25	1.50	1.00
36–44	FC/DH	coarse/very coarse	1	1	0.75	3.50	1.50
44–48	DH	very coarse	1	1	1.00	4.00	2.00
48–52	DH/MF	very coarse	6	1	0.75	3.50	2.50
52–56	DH	very coarse	1	1	0.50	4.00	3.00

Appendix 9. Snow stratigraphy of S5, sampled on 10 April 2013, in SoS2013; n/a = not available.

Temperature		Density		EC		
Depth (cm)	°C	Depth (cm)	g cm^{-3}	Depth (cm)	ng g^{-1}	ng cm^{-3}
air	0.7	0–5	0.168	0–5	1690	374
0	0.1	5–10	0.224			
6	–1.1	10–15	0.308			
16	–5.6	15–20	0.256			
26	–5.7	20–25	0.224			
36	–5.3	25–30	0.320			
46	–4.4	30–35	0.276			
56	–3.7	35–40	0.248			
		40–45	0.264			
		45–50	n/a			
		50–56	n/a			

Appendix 10. Snow stratigraphy of S7, sampled on 10 April 2013, in SoS2013.

Depth (cm)	Grain shape	Size	Hardness	Wetness	Grain size (mm)		
					Min	Max	Mean
0–1	MFcr	coarse	5	1	0.75	1.50	1.00
1–2.5	FCxr	coarse	1	1	0.50	1.75	1.25
2.5–3	MFcr	coarse	3	1	1.00	1.50	1.25
3–12.5	Fcxr	coarse	1	1	0.50	1.50	0.75
12.5–13	MFcr	medium	5	1	0.25	1.50	0.75
13–16.5	FCxr	medium	1	1	0.50	1.50	0.75
16.5–25.5	DHxr	coarse/very coarse	1	1	0.75	3.00	2.00
25.5–36.5	DHxr	medium/coarse	3	1	0.50	2.50	1.25
36.5–46.5	DHcp	very coarse	2	1	1.25	4.00	2.00

Appendix 11. Snow stratigraphy of S7, sampled on 10 April 2013, in SoS2013; n/a = not available.

Temperature		Density		EC		
Depth (cm)	°C	Depth (cm)	g cm^{-3}	Depth (cm)	ng g^{-1}	ng cm^{-3}
air	–0.6	0–5	n/a	0–5	1470	323
0	–3.7	5–10	0.252			
6.5	–4.4	10–15	0.252			
16.5	–6.2	15–20	0.224			
26.5	–6.0	20–25	0.224			
36.5	–5.1	25–30	0.292			
46.5	–4.2	30–35	0.296			
		35–40	0.22			
		40–45	0.26			

Appendix 12. Reference snow pit observed on 17 April 2013, in SoS2013.

Depth (cm)	Grain shape	Size	Hardness	Wetness	Grain size (mm)		
					Min	Max	Mean
0–2	MFcl	coarse	1	3	0.50	1.25	1.00
2–32	MFcl	coarse	1	3	0.75	2.00	1.25
32–34	MFcr	very coarse	6	1	0.50	2.50	1.50
34–38	MFcl	very coarse	1	3	0.50	2.50	1.25

Appendix 13. Reference snow pit (continued) observed on 17 April 2013, in SoS2013; n/a = not available.

Temperature		Density		EC		
Depth (cm)	°C	Depth (cm)	g cm^{-3}	Depth (cm)	ng g^{-1}	ng cm^{-3}
air	2.9	0–5	0.420	0–5	134	52.2
0	0.1	5–10	0.382	5–10	55.3	21.1
8	0.0	10–15	0.392	10–15	87.9	34.4
18	0.0	15–20	0.372	15–20	n/a	n/a
28	0.0	20–25	0.396	20–25	n/a	n/a
38	0.0	25–30	0.400			
		30–38	0.496			

Appendix 14. Snow stratigraphy of S5 on 17 April 2013, in SoS2013; n/a = not available.

Depth (cm)	Grain shape	Size	Hardness	Wetness	Grain size (mm)		
					Min	Max	Mean
0–1	MFcl	coarse	1	3	0.75	1.50	1.00
1–16	MFcl	coarse	1	3	0.50	1.50	1.25
16–25	MFcl	very coarse	1	3	1.00	4.00	2.50
25–29	MFcl	very coarse	1	3	1.00	3.00	2.00
29–30	IFil	n/a	6	1			n/a
30–33	Mfsl	n/a	1	n/a	0.75	2.00	1.00

Appendix 15. Snow stratigraphy of S5 (continued) on 17 April 2013, in SoS2013; n/a = not available.

Temperature		Density		EC		
Depth (cm)	°C	Depth (cm)	g cm^{-3}	Depth (cm)	ng g^{-1}	ng cm^{-3}
air	3.2	0–5	0.384	0–5	730	233
0	0.1	5–10	0.388	5–10	118	24.3
3	0.0	10–15	0.396	10–15	88.4	0.559
13	0.0	15–20	0.404	15–20	64.5	n/a
23	0.0	20–25	0.392	20–25	55.9	n/a
33	0.0	25–33	0.608			

Appendix 16. Snow stratigraphy of S7 on 17 April 2013, in SoS2013; n/a = not available.

Depth (cm)	Grain shape	Size	Hardness	Wetness	Grain size (mm)		
					Min	Max	Mean
0–2	MFcl	coarse	1	3	0.50	1.50	1.00
2–17	MFcl	coarse	1	3	0.50	1.50	1.25
17–26	MFcl	very coarse	1	3	0.50	3.00	2.00
26–32	MFpc/cl	very coarse	4	2	1.00	3.00	2.00
32–33	IF	n/a	6	1	n/a	n/a	n/a
33–35	MFsl	n/a	1	5	n/a	n/a	n/a

Appendix 17. Snow stratigraphy of S7 (continued) on 17 April 2013, in SoS2013; n/a = not available.

Temperature		Density		EC		
Depth (cm)	°C	Depth (cm)	g cm^{-3}	Depth (cm)	ng g^{-1}	ng cm^{-3}
air	3.2	0–5	0.368	0–5	529	154
0	0.0	5–10	0.384	5–10	6.98	–18.4
5.0	0.0	10–15	0.404	10–15	5.27	–32.3
15.0	0.0	15–20	0.36	15–20	n/a	n/a
25.0	0.0	20–25	0.416	20–25	n/a	n/a
35.0	–0.1	25–30	0.708	25–30	n/a	n/a
		30–35	n/a			